consumption of surface materials cannot be ruled out, but the apparent lack of convergence zones is one of several important differences between plate tectonics on Earth and what has been seen so far of plate movement and dark band growth on Europa.

Even without surface signatures of plate convergence, could the ~100-km spacing of the more prominent dark bands (Fig. 1) be a result of subsurface convection that does not, or did not, involve recycling of surface materials? If so, this would be on a different scale to solid-state convection proposed near Conamara Chaos[7]. In that area Pappalardo et al.[7] conclude that domes, dark spots, and pits are evidence for thermally driven vertical movements 7–15 km in diameter and 5–20 km apart in the near-subsurface. Domes, dark spots, and pits are much less pervasive among the dark wedge bands discussed here, suggesting that heat transfer from the interior occurred differently in this area. Although a water-ice-rich layer >50 km thick is allowed by several analyses that assume differentiation and segregation of water from a deeper silicate mantle[8,9], as well as interior models based on gravitational data derived from Doppler tracking of the Galileo spacecraft[10], the idea that these materials are organized into a network of ~100-km convection cells causing dark band formation is inconsistent with the existence of isolated dark wedge bands (for example, near 52° N, 230° W).

A more likely explanation is that plate fracturing and movement in response to regional surface stresses simply allowed material to rise passively to the surface to form the dark bands. A very densely fractured region centred at 40° S, 205° W is partly surrounded by bright plains with prominent dark bands showing evidence of plate offsets[1–3,11–13] (Fig. 1). This annulus includes the disrupted zone seen by Galileo on its first and fourth orbits and the dark bands seen at higher resolution on the third orbit. Destruction of surface material in the area of 40° S, 205° W could have provided room in surrounding terrain for icy plates to separate and rotate relative to one another, with emplacement of dark band material between the plates occurring in response to these motions. The very densely fractured region in the centre of the annulus has not been seen yet at high resolution, so the cause of the dense fracturing and the fate of the original surface materials cannot be determined. Localized heating similar to that proposed for the Conamara Chaos region[6] is a likely possibility. We conclude that creation of dark bands during plate separation is a result of regional surface stresses opening pre-existing fractures which sub-surface materials exploit incrementally. □

1. Schenk, P. M. & Seyfert, C. K. Fault offsets and proposed plate motions for Europa. *Eos* **61**, 286 (1980).
2. Schenk, P. M. & McKinnon, W. B. Fault offsets and lateral crustal movement on Europa: Evidence for a mobile ice shell. *Icarus* **79**, 75–100 (1989).
3. Golombek, M. P. & Banerdt, W. B. Constraints on the subsurface structure of Europa. *Icarus* **83**, 441–452 (1990).
4. Belton, M. J. S. *et al*. Galileo's first images of Jupiter and the Galilean satellites. *Science* **274**, 377–385 (1996).
5. Tufts, B. R., Greenberg, R., Sullivan, R., Pappalardo, R. & the Galileo Imaging Team Reconstruction of Europan terrain in the Galileo C3 "wedges" image and its geological implications. *Lunar Planet. Sci. Conf.* **XXVIII**, 1455–1456 (1997).
6. Carr, M. H. *et al*. Evidence for a subsurface ocean on Europa. *Nature* **391**, 363–365 (1998).
7. Pappalardo, R. T. *et al*. Morphological evidence for solid-state convection in Europa's ice shell. *Nature* **391**, 365–368 (1998).
8. Fanale, F. P., Johnson, T. V. & Matson, D. L. in *Planetary Satellites* (ed. Burns, J. A.) 379–405 (Univ. Arizona Press, Tucson, 1977).
9. Squyres, S. W., Reynolds, R. T., Cassen, P. M. & Peale, S. J. Liquid water and active resurfacing on Europa. *Nature* **301**, 225–226 (1983).
10. Anderson, J. D., Lau, E. L., Sjogren, W. L., Schubert, G. & Moore, W. B. Europa's differentiated internal structure: Inferences from two Galileo encounters. *Science* **276**, 1236–1239 (1997).
11. Tufts, B. R. Photogeological analysis of Europan tectonic features. *Lunar Planet Sci. Conf.* **XXIV**, 1445–1446 (1993).
12. Tufts, B. R. A San Andreas-sized strike-slip fault on Europa. *Lunar Planet Sci. Conf.* **XXVII**, 1343–1344 (1996).
13. Pappalardo, R. T. & Sullivan, R. Evidence for separation across a gray band on Europa. *Icarus* **123**, 557–567 (1996).

Correspondence and requests for materials should be addressed to R.S. (e-mail: sullivan@cuspif.tn. cornell.edu).

Transport properties governed by surface barriers in Bi2Sr2CaCu2O8

Dan T. Fuchs*, Eli Zeldov*, Michael Rappaport†, Tsuyoshi Tamegai‡, Shuuichi Ooi‡ & Hadas Shtrikman*

* *Department of Condensed Matter Physics,* † *Physics Services, The Weizmann Institute of Science, Rehovot 76100, Israel*
‡ *Department of Applied Physics, The University of Tokyo, Hongo, Bunkyo-ku, Tokyo 113, Japan*

One of the most common investigation techniques of type-II superconductors is the transport measurement, in which an electrical current is applied to a sample and the corresponding resistance is measured as a function of temperature and magnetic field. At temperatures well below the critical temperature, T_c, the resistance of a superconductor is usually immeasurably low. But at elevated temperatures and fields, in the so-called vortex liquid phase, a substantial linear resistance is observed[1]. In this dissipative state, which in anisotropic high-temperature superconductors like $Bi_2Sr_2CaCu_2O_8$ may occupy most of the mixed-state phase diagram, the transport current is usually assumed to flow uniformly across the sample as in a normal metal. To test this assumption, we have devised a measurement approach which allows determination of the flow pattern of the transport current across the sample. The surprising result is that, in $Bi_2Sr_2CaCu_2O_8$ crystals, most of the current flows at the edges of the sample rather than in the bulk, even in the highly resistive state, due to the presence of strong surface barriers. This finding has significant implications for the interpretation of existing resistivity data and may be of importance for the development of high-temperature superconducting wires and tapes.
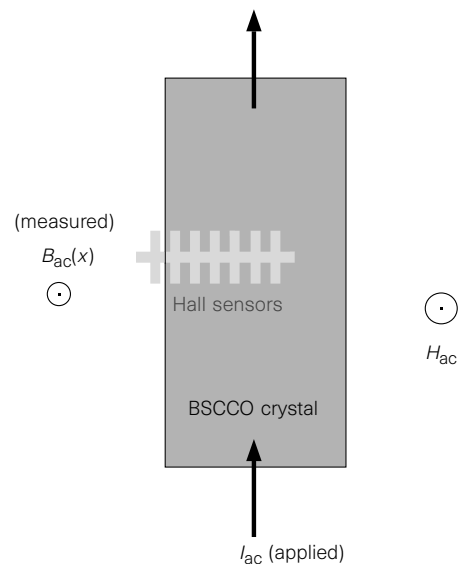
Figure 1 Experimental set-up. A schematic top view of $Bi_2Sr_2CaCu_2O_8$ crystal (1.5 × 0.15 × 0.01 mm) attached to an array of seven GaAs/AlGaAs two-dimensional electron-gas Hall sensors underneath the sample. The sensors have an active area of $10 \times 10\,\mu m^2$ and are 10 μm apart. There is one sensor outside the sample; the other six span more than half of the sample width. Magnetic field H_{dc} is applied perpendicular to the sample surface. An a.c. current I_{ac} is applied to the crystal through electrical contacts. The sensors are used to probe the perpendicular component of the self-induced a.c. field, B_{ac}, generated by the a.c. current.

The experiments were carried out on several $Bi_2Sr_2CaCu_2O_8$ (BSCCO) crystals ($T_c \approx 88$ K) with typical dimensions of $1.5 \times 0.15 \times 0.01$ mm. The crystals were attached directly to the surface of a linear Hall-sensor array consisting of seven 10×10 μm sensors as shown schematically in Fig. 1. A d.c. magnetic field, H_{dc}, was applied perpendicular to the surface (parallel to the c-axis of the crystal). A low-frequency (65–400 Hz) a.c. current, I_{ac}, in the range 0.4–10 mA (r.m.s.), was applied to the sample using gold contacts. The findings described below are independent of the frequency and the amplitude of I_{ac}, and so only data obtained for 4 and 10 mA at 72.8 Hz are presented. In this study, we have used a sensitive a.c. technique to measure the field profile $B_{ac}(x)$ across the sample, where $B_{ac}(x)$ is the self-induced field of the transport current I_{ac}. This method differs from the measurements of $B_{dc}(x)$ induced by H_{dc} which provide valuable information about the local magnetization or susceptibility of the sample[2,3]. The present study requires high resolution because B_{ac} is of the order of 0.1 G as compared to the typical B_{dc} of 1,000 G. The use of the a.c. mode provides the necessary separation between the field B_{ac} due to transport current, and the field B_{dc} due to the applied field. The transport-current distribution across the sample is then determined from the experimental $B_{ac}(x)$ profiles.

In a highly dissipative state, the current is expected to flow uniformly across the sample as in a normal conductor, as shown on the left in Fig. 2a. In this case, the resulting vertical component of the self-induced field is given by the solid curve on the right in Fig. 2a, as calculated using the Biot–Savart law[4]. At low temperatures, on the other hand, material disorder pins the vortices and prevents their motion, resulting in a finite critical current. In this case the transport current is expected to flow in a way similar to the case of the Meissner state where $B_{ac}(x)$ is expelled from the sample[5,6] as shown in Fig. 2c. As the superconductor is cooled down in the presence of H_{dc}, a monotonic increase of the critical current is expected and therefore a gradual transition from B_{ac} of Fig. 2a to Fig. 2c should occur[5,6].

Yet there is another important mechanism, the Bean–Livingston surface barrier[7], which is usually not taken into account in transport studies. Here we use the term surface barrier to refer to both the Bean–Livingston and a similar geometrical barrier mechanism[8]. Because the presented data are mainly for $H_{dc} > H_{c1}(T)$ (the lower critical field), the contribution of the geometrical barrier is negligible in this case. In order to enter or leave a superconductor, a vortex has to overcome a potential barrier at the surface. This barrier is the result of competition between two forces acting on the vortex near a parallel surface: an inward force due to the presence of the shielding currents, and an outward force due to the attraction between the vortex and its fictitious mirror image outside the sample. In the presence of significant surface barrier, the transport current flows at the edges of the sample, where the vortices enter and leave the superconductor, in order to drive the vortices over the barrier. $B_{ac}(x)$, calculated assuming that the entire current flows at the edges, is shown by the solid curve in Fig. 2b. This field profile is quite different from that of the uniform flow in Fig. 2a. In particular, the signs of $B_{ac}(x)$ within the sample are opposite.

It has been shown that surface barriers have an important contribution to the hysteretic magnetization of clean high-T_c superconductors[9–11]. These barriers govern the magnetization below the so-called irreversibility line. Owing to practical sensitivity limitations, transport measurements are usually carried out above this irreversibility line where the magnetization is reversible and
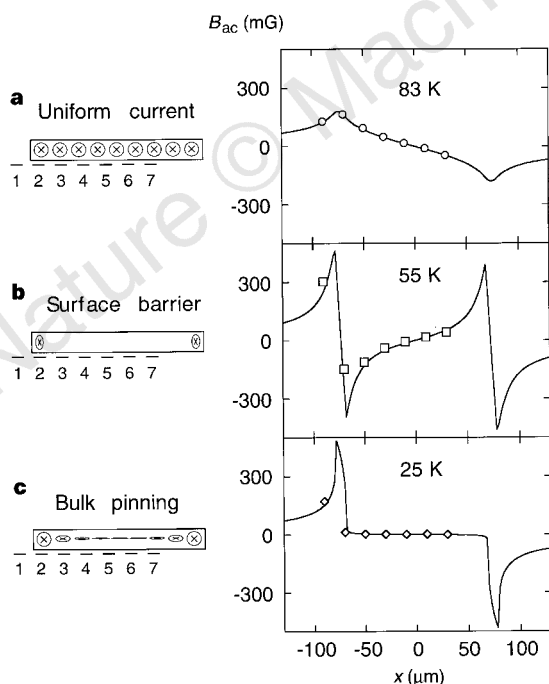
Figure 2 Schematic cross-section of the sample with the attached Hall sensors (left) and the corresponding field profiles $B_{ac}(x)$ at three temperatures (right). Open symbols are the self-field measured by the sensors ($H_{dc} = 1,000$ G, $I_{ac} = 4$ mA), and the solid lines are the calculated field profiles for 4 mA current using the Biot–Savart law. **a**, At elevated temperatures, the current flows uniformly across the sample. **b**, At intermediate temperatures practically all the current flows at the edges of the superconductor owing to surface barriers. In this case the field inside the sample has an inverted profile relative to the uniform-current-flow case. **c**, At low temperatures, strong bulk pinning is present which results in zero B_{ac} within the sample.
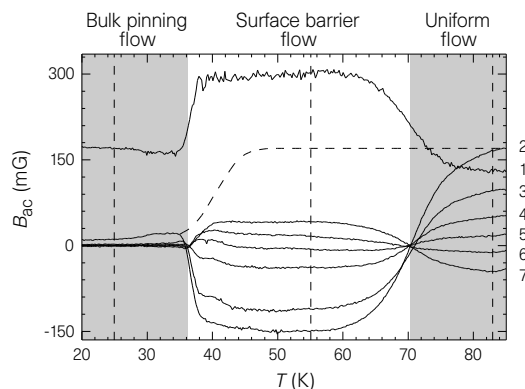
Figure 3 Self-induced field $B_{ac}(x)$ generated by 4 mA a.c. current as a function of the temperature during cooling of the $Bi_2Sr_2CaCu_2O_8$ crystal in a field $H_{dc} = 0.1$ T. The curves are labelled according to the sensor numbers as indicated in Fig. 2. The vertical dashed lines mark the temperatures for which the B_{ac} values are plotted as a function of the sensor location in Fig. 2. At elevated temperatures the current flows rather uniformly across the sample (83 K profile in Fig. 2a). Surface barriers dominate the vortex dynamics over a wide range of intermediate temperatures where the currents flow at the edges of the sample (55 K profile in Fig. 2b). At the crossing point at 70 K, half of the current flows in the bulk and half at the edges causing cancellation of the field in the central part of the sample (superposition of profiles **a** and **b** of Fig. 2). At low temperatures, strong bulk pinning prevents vortex motion, resulting in zero B_{ac} in the sample. The dashed curve indicates the expected field at sensor 2 if the current flow were governed by the bulk vortex properties as commonly assumed. The observed inversion of the field profile is caused by the dominant role of surface barriers.

hence surface effects are expected to be of no importance. The effect of surface barriers on transport measurements has been considered theoretically[12], and some studies have suggested that surface barriers may be of significance[13], in particular as a source of voltage noise[14,15]. The flow patterns of the transport current have been tested in several investigations of thin films and tapes[16–19] but these studies have focused on the critical state behaviour and sample inhomogeneities rather than on surface barriers.

Figure 3 shows the self-field B_{ac} as measured by the sensors on cooling the BSCCO crystal in $H_{dc} = 0.1\,T$ and $I_{ac} = 4\,mA$. The curves are labelled by the sensor number as indicated in the left-hand side of Fig. 2. At elevated temperatures, $B_{ac}(x)$ decreases monotonically across the sample (sensors 2–7) owing to a uniform transport current. The measured field profile at 83 K is shown in Fig. 2a (right) by the open symbols, along with the calculated field profile for 4 mA uniform current shown by the solid curve. The fit clearly indicates that at high temperatures the transport current flows uniformly across the width of the crystal. At low temperatures, $T < 36\,K$ in Fig. 3, $B_{ac}(x)$ is finite only outside the bulk of the sample (sensor 1, and sensor 2 which is close to the edge) and is zero inside the sample. This behaviour indicates strong bulk pinning and a finite critical current. Figure 2c (right) shows the measured field profile at 25 K and the corresponding calculated curve for this case. At intermediate temperatures, if the surface barrier is neglected, one expects a gradual crossover from a uniform current flow to bulk pinning as indicated by the dashed line for sensor 2 in Fig. 3. However, the measured B_{ac} is drastically different and displays a negative signal which cannot be explained by any model based on bulk vortex properties. This inversion of the polarity of B_{ac} at $T = 70\,K$ for all sensors within the sample is the result of current flow at the edges of the sample due to the presence of surface barriers. The measured field profile at $T = 55\,K$ is shown in Fig. 2b (right). The solid curve is calculated for the 4 mA current flowing entirely at the edges of the sample. The clear agreement with the data indicates that the surface barrier completely dominates the vortex dynamics, and as a result, practically the entire current, within experimental resolution of few per cent, flows at the edges of the

sample. Figure 3 shows that at high temperatures the current flows uniformly, then crosses over to a complete surface flow over a wide range of temperatures, and finally changes to bulk-pinning-like flow only at low temperatures.

The above results have important implications for the interpretation of transport measurements. Figure 4 shows the resistance transition in the same BSCCO crystal at various applied fields. Such measurements are usually interpreted in terms of bulk resistivity caused by, for example, viscous vortex flow or pinning. Apparently, only the very top region of our data, where the current flows uniformly in the bulk (dark lines in Fig. 4), reflects bulk vortex properties. Most of the data shown by the grey lines, however, do not reflect bulk vortex properties but rather the properties of the surface barrier. The situation can be roughly represented by the two equivalent circuits at the top of Fig. 4. At elevated temperatures, the sample can be regarded as a uniform resistor. But at lower temperatures (grey lines) the surface barriers act as low resistance shunts, and hence practically all the current flows at the edges. As a result, the total measured resistance is that of the surface barrier rather than that of the bulk.

An alternative way of describing the process is by noting that the measured resistance always reflects the flow rate of the vortices across the sample. However, the flow rate, rather than being determined by bulk vortex pinning and viscous drag, is determined by the hopping rate over the surface barrier[12]. This activation is the rate-limiting process impeding vortex motion. Vortex flow rate over the barrier has to be equal to that in the bulk. As a result practically all of the current flows at the edges in order to provide the large force required to overcome the barrier, while only a very small fraction of the current flows in the bulk in order to overcome the small bulk viscous drag. The apparent measured resistance is thus orders of magnitude lower than the true bulk resistance. In other words, the vortices in the bulk are much more mobile, and the corresponding viscous drag coefficient and the pinning force are much smaller, than what is usually deduced from transport measurements[20–23].

In addition, resistance of BSCCO crystals commonly displays thermally activated Arrhenius behaviour. In view of the work reported here, such Arrhenius behaviour is caused by the thermal activation over the surface barrier[12] and does not reflect the bulk pinning, as is usually interpreted[20,21]. Another interesting observation is the recently reported sharp drop in resistance at the first-order vortex lattice melting transition in BSCCO[23–25], which is seen, for example, in the 300 Oe data in Fig. 4 at about 65 K. Such a drop is usually ascribed to the sharp onset of bulk pinning on solidification of the lattice[26,27]. Analysis of the temperature dependence of the current distribution at 300 Oe indicates that even this feature mainly reflects a sharp change in the surface rather than bulk properties, as most of the current still flows at the edges of the crystal and the vortices are unpinned both above and below the melting transition. This does not mean that the bulk properties do not change, but rather that the transport measurements do not probe the true bulk vortex dynamics at the transition. Finally, several magneto-optical investigations have shown that, in BSCCO tapes and wires, the current distribution often peaks at the interface between the superconducting filaments and the Ag sheath rather than within the bulk of the filaments[19]. It is thus possible that the surface barriers are also of importance to the current-carrying capability of the commercial wires in a way similar to the behaviour of the single crystals. □
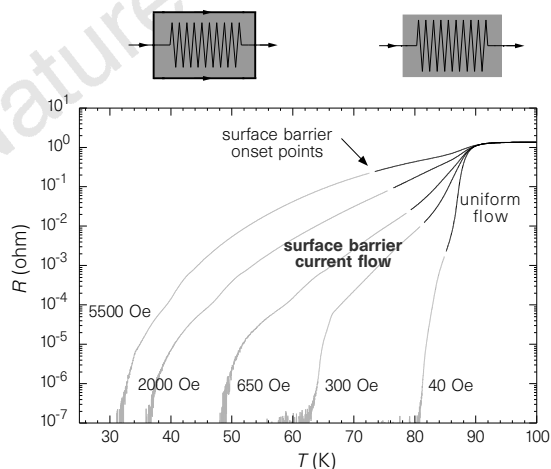
Figure 4 Resistance of $Bi_2Sr_2CaCu_2O_8$ crystal as a function of temperature at the indicated applied fields ($I_{ac} = 10\,mA$). Only in the region of the black curves does the current flow uniformly across the sample (at least 90% of the current). In the region where the curves are grey most of the current flows at the edges of the sample owing to strong surface barriers. The top left diagram illustrates how the surface barriers shunt the current flow in a large part of the phase diagram (surface barrier flow region in Fig. 3), and as a result the measured resistance may be orders of magnitude lower than the true bulk resistance of the superconductor. The top right diagram illustrates the uniform flow case where the surface barriers are unimportant.

1. Huse, D. A., Fisher, P. A. & Fisher, D. S. Are superconductors really superconducting? *Nature* **358**, 553–559 (1992).
2. Zeldov, E. *et al*. Thermodynamic observation of first-order vortex-lattice melting transition. *Nature* **375**, 373–376 (1995).
3. Fuchs, D. T. *et al*. Simultaneous resistivity onset and first-order vortex-lattice phase transition in $Bi_2Sr_2CaCu_2O_8$. *Phys. Rev. B* **54**, R796–R799 (1996).
4. Purcell, E. M. *Electricity and Magnetism* (McGraw-Hill, Singapore, 1985).
5. Brandt, E. H. & Indenbom, M. Type-II-superconductor strip with current in perpendicular magnetic field. *Phys. Rev. B* **48**, 12893–12906 (1993).

6. Zeldov, E., Clem, J. R., McElfresh, M. & Darwin, M. Magnetization and transport currents in thin superconducting films. *Phys. Rev. B* **49,** 9802–9822 (1994).

7. Bean, C. P. & Livingston, J. D. Surface barriers in Type-II superconductors. *Phys. Rev. Lett.* **12,** 14–16 (1964).

8. Zeldov, E. *et al.* Geometrical barriers in high-temperature superconductors. *Phys. Rev. Lett.* **73,** 1428–1431 (1994).

9. Chikumoto, N., Konczykowski, M., Motohira, N. & Malozemoff, A. P. Flux-creep crossover and relaxation over surface barriers in $Bi_2Sr_2CaCu_2O_8$ crystals. *Phys. Rev. Lett.* **69,** 1260–1263 (1992).

10. Konczykowski, M., Burlachkov, L. I., Yeshurun, Y. & Holtzberg, F. Evidence for surface barriers and their effect on irreversibility and lower critical field measurements in Y-B-CU-O crystals. *Phys. Rev. B* **43,** 13707–13710 (1991).

11. Zeldov, E. *et al.* Nature of the irreversibility line in $Bi_2Sr_2CaCu_2O_8$. *Europhys. Lett.* **30,** 367–372 (1995).

12. Burlachkov, L., Koshelev, A. E. & Vinokur, V. M. Transport properties of high temperature superconductors: Surface vs bulk effect. *Phys. Rev. B* **54,** 6750–6757 (1996).

13. White, W. R., Kapitulnik, A. & Beasley, M. R. Collective vortex motion in a-MoGe superconducting thin-films. *Phys. Rev. Lett.* **70,** 670–673 (1993).

14. D'Anna, G. *et al.* Vortex-motion-induced voltage noise in $YBa_2Cu_3O_{7-d}$ single crystals. *Phys. Rev. Lett.* **75,** 3521–3524 (1995).

15. Gordeev, S. N. *et al.* Current-induced organization of vortex motion in Type-II superconductors. *Nature* **385,** 324–326 (1997).

16. Manhart, J. *et al.* Spatially resolved observation of supercurrents across grain boundaries in YBaCuO films. *Science* **245,** 839–841 (1989).

17. McElfresh, M. *et al.* Local time dependent magnetization of superconducting films in presence of transport current. *Phys. Rev. B* **51,** 9111–9117 (1995).

18. Indenbom, M. V., Forkl, A., Kronmüller, H. & Habermeier, H.-U. Critical-current in YBCO thin-film bridge studied using magnetooptic technique. *J. Supercond.* **6,** 173–178 (1993).

19. Welp, U. *et al.* Imaging of transport currents in superconducting (Bi, Pb)₂Sr₂Cu₃Oₓ composites. *Nature* **376,** 44–46 (1995).

20. Palstra, T. T. M., Batlogg, B., Schneemeyer, L. F. & Waszczak, J. V. Thermally activated dissipation in $Bi_{2.2}Sr_2Ca_{0.8}Cu_2O_{8+\delta}$. *Phys. Rev. Lett.* **61,** 1662–1665 (1988).

21. Busch, R., Ries, G., Werthner, H., Krieselmayer, G. & Saemann-Ischenko, G. New aspects of the mixed state from 6-terminal measurements on $Bi_2Sr_2CaCu_2O_x$ single-crystals. *Phys. Rev. Lett.* **69,** 522–525 (1992).

22. Koshelev, A. E. Mechanism of thermally activated c-axis dissipation in layered high-Tc superconductors at high fields. *Phys. Rev. Lett.* **76,** 1340–1343 (1996).

23. Tsuboi, T., Hanaguri, T. & Maeda, A. Nature of the vortex liquid in $Bi_2Sr_2CaCu_2O_y$. *Phys. Rev. B* **55,** R8709–R8712 (1997).

24. Watauchi, S. *et al.* Observation of resistivity drops and the vortex phase-diagram in $Bi_2Sr_2CaCu_2O_y$. *Physica C* **259,** 373–378 (1996).

25. Fuchs, D. T. *et al.* Resistive evidence for vortex-lattice sublimation in $Bi_2Sr_2CaCu_2O_8$. *Phys. Rev. B* **55,** R6156–R6159 (1997).

26. Safar, H., Gammel, P. L., Huse, D. A. & Bishop, D. J. Experimental-evidence for a 1ˢᵗ-order vortex-lattice-melting. *Phys. Rev. Lett.* **69,** 824–827 (1992).

27. Kwok, W. K. *et al.* Vortex lattice melting in untwinned and twinned single-crystals of $YBa_2Cu_3O_{7-\delta}$. *Phys. Rev. Lett.* **69,** 3370–3373 (1992).

Icosahedral packing of B₁₂ icosahedra in boron suboxide (B₆O)

Hervé Hubert*, Bertrand Devouard†‡, Laurence A. J. Garvie†, Michael O'Keeffe*, Peter R. Buseck†, William T. Petuskey* & Paul F. McMillan*

* *MRSEC, Department of Chemistry & Biochemistry, Arizona State University, Tempe, Arizona 85287, USA*

† *Departments of Geology and Chemistry & Biochemistry, Arizona State University, Tempe, Arizona 85287, USA*

Objects with icosahedral symmetry (I_h) bear a special fascination; natural examples are rare, but include radiolaria[1] and virus particles (virions)[2]. The discovery[3] of C_{60}, a molecule in the shape of a truncated icosahedron with I_h symmetry, has aroused widespread interest. In 1962, Mackay[4] described a radiating packing of spheres in I_h symmetry, in which the centres of successive shells of spheres lie on the surfaces of icosahedra. There has been extensive investigation of the conditions under which such packing might be realized in assemblies of atoms or of

‡ Present address: Département de Géologie, UMR 6524 Magmas et Volcans, 5, rue Kessler, F-63038 Clermont-Ferrand cedex, France.

molecules such as C_{60} (ref. 5). Here we report the preparation, at high temperatures and pressures, of boron suboxide (B_6O) in which the preferred form of the material is as macroscopic, near-perfect, regular icosahedra, similar to the multiply-twinned particles observed in some cubic materials. A major difference is that B_6O has a rhombohedral structure that nearly exactly fits the geometrical requirements needed to obtain icosahedral twins. These icosahedral particles have a structure that can be described as a Mackay packing of icosahedral B_{12} units, and thus has long-ranged order without translational symmetry.

The icosahedron (regular polyhedron with 20 triangular faces) is a forbidden morphology for single crystals: because of the absence of 5-fold axes in classical crystallography, the external forms of single crystals cannot exhibit such symmetry. However, some 'crystalline' objects without three-dimensional periodicity do not comply with this rule: in chrysotile and polygonal serpentine minerals, the fibre axis has 5-fold symmetry[6,7]. Five-fold cyclic twins, usually imperfect, have long been known in minerals such as cassiterite (SnO_2), pentagonite[8] or diamond[9,10]. Small multiply-twinned particles (MTPs) are known with the form of pentagonal bipyramids (decahedra), and also, rarely, as icosahedra of elemental metals[11–13] and of chemical-vapour-deposited (CVD) diamond[14]. Many quasicrystals have icosahedral space-group symmetry and, in some cases, crystallize in pentagonal dodecahedra[15] and rhombic triacontahedra[16] with icosahedral symmetry.
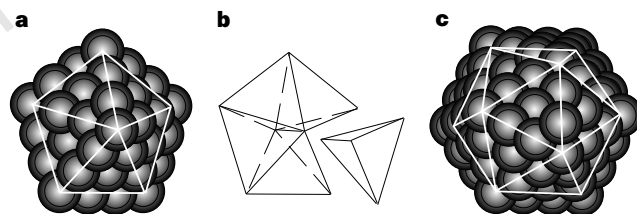
Figure 1 a, An element of decagonal sphere packing. **b**, A decagon (pentagonal bipyramid) with one of its five component tetrahedra removed. **c**, An element of icosahedral (Mackay) sphere packing. The tetrahedra in c.c.p. metals are derived from the familiar 'pile-of-cannonballs' densest packing of atoms with density ρ_{cp}. The density of the decagonal sphere packing[31] is a maximum if the tetrahedra are distorted so that the length of the edge common to the five tetrahedra is increased by a factor of $\sqrt{3}\sin(\pi/5) = 1.018$. The packing density is then $0.991\rho_{cp}$ (**a**). Thus only a small strain is required to produce decahedral multiply-twinned particles (MTPs) from cubic parent material[9,11,12]. Icosahedral MTPs consist of 20 tetrahedra meeting at a vertex; the tetrahedra must be more distorted from ideality, as described in the text. The density of the sphere packing is now $5/(2\sqrt{(5+\sqrt{5})})\rho_{cp} = 0.929\rho_{cp}$ (ref. 4).
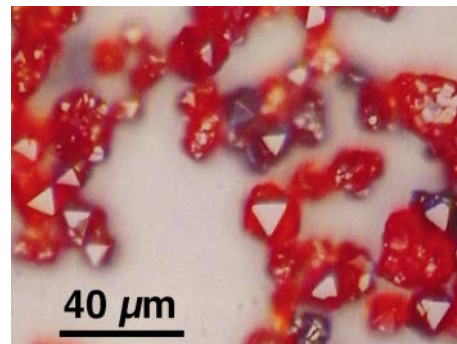
Figure 2 Reflected-light optical image of B_6O icosahedral particles. Triangular faces of individual icosahedra are evident. Individual particles occur as isolated or clustered icosahedra, although rounded particles of very fine-grained sintered material also exist. The colour is consistent with a bandgap around 2 eV (ref. 32).